Chemical Physics Letters 539–540 (2012) 133–138

Contents lists available at SciVerse ScienceDirect

Chemical Physics Letters

journal homepage: www.elsevier.com/locate/cplett

Carrier recombination dynamics through defect states of ZnO nanocrystals: From nanoparticles to nanorods

Arunasish Layek [a], Biswajit Manna [a,1], Arindam Chowdhury [a,b,*]

[a] Department of Chemistry, Indian Institute of Technology Bombay, Powai, Mumbai 400 076, India
[b] National Centre for Photovoltaic Research and Education, Indian Institute of Technology Bombay, Powai, Mumbai 400 076, India

ARTICLE INFO

Article history:
Received 6 February 2012
In final form 14 May 2012
Available online 23 May 2012

ABSTRACT

Time-resolved photoluminescence spectroscopy has been used to probe carrier relaxation dynamics of defect emission from ZnO nanostructures of different size and shape. The radiative recombination through the trap states is found to slow down continuously with increasing particle diameters ($\leqslant$5 nm) and shows saturation behaviors for larger particles. Intriguingly, the photoluminescence decay for nanorods is observed to be considerably faster as compared to nanoparticles of comparable diameters, which is more apparent for lower energy decays. This effect is assigned to modulation of defect densities and appearance of topological surface states upon shape transitions of spherical nanoparticles to anisotropic nanorods.

1. Introduction

Nanometer-size semiconductor particles, rods, nanobelts, wires, tubes, and tetrapods exhibit electronic and optical properties that depend on their size, shape, and surface morphology [1]. Zinc oxide is one of the important semiconductor oxide materials, with direct wide band gap (3.37 eV) and large exciton binging energy (60 meV), and have tremendous applications in nanoscale electronic and photonic devices applications [2–4]. However, nanocrystalline ZnO severely suffer from the drawbacks of multiple surface related [5] and internal bulk defects [6] which drastically limit its applications. In the past decade, various chemical and physical methods used to produce ZnO nanocrystals (NCs) have been found to show strong visible emission (in the green-yellow-orange region) associated with surface defects, [7–8] in addition to the expected excitonic transitions in the UV ($\geqslant$3.2 eV). Although the exact nature of the associated defects are still ambiguous, it is generally believed that intrinsic defects like oxygen vacancy, zinc vacancy, and other surface related defects like dangling bonds, hydroxo or peroxo linkages are responsible for the visible PL emission [9–12]. It has been shown that the broad visible emission band and the narrow near-band gap (NBG) UV emission arise from competing radiative recombination process; the visible emission is prominent due to efficient carrier recombination through defect mediated trap states, while crystalline regularity augments the intensities of NBG emission while simultaneously lowering the efficiency of visible emission. The relative intensities of the NBG and visible emission has been shown to depend on the size, shape, surface states and defect density in the nanostructures [13–15].

In ZnO nanostructures, while the visible emission is undesirable for near-UV emitting devices, the defect luminescence, which is predominant in most nanoscale ZnO materials, has importance in applications like gas sensing [16], catalysis [1], cell-labeling [17], and high efficiency green phosphor [18]. Therefore, investigating the nature of surface related defects is of immense interest for both fundamental scientific point of view and for further development of various nanostructures in accordance with their applications, such as those using spherical nanoparticles (NPs) and 1-D nanorods (NRs). It is therefore important to understand free carrier mobility and carrier-recombination lifetimes in such nanostructures since they produce sub-band gap states which function as energetic traps for charge carriers (electrons or holes) [19]. In this context, shape, size and exposed surface of semiconductor nanomaterials have a decisive role in the PL emission behaviors [3,13,20]. Even though there are several reports on the NBG charge carrier dynamics (in the UV) for ZnO NCs of different shapes (such as spherical particles, 1-D wires/rods, tetrapods etc.) [3,21], studies on the radiative recombination dynamics mediated by the defect states (i.e. in visible region) is far less prevalent. Recently, the defect related emission has been studied by Zhang et al. [13] wherein the visible luminescence mechanism for ZnO was shown to be dependent on both crystal size as well as type and density of defects. On the other hand, Mehl et al. [22] have studied local nanoenvironment dependent defect dynamics within single ZnO microrods, which further demonstrated that the ends of the rods display diverse carrier recombination dynamics as compared to

* Corresponding author at: Department of Chemistry Indian Institute of Technology Bombay, Powai, Mumbai 400 076, India. Fax: +912225767152.
E-mail address: arindam@chem.iitb.ac.in (A. Chowdhury).
[1] Present address: Radiation and Photochemistry Division, Bhabha Atomic Research Centre, Trombay, Mumbai 400 085, India.

0009-2614/$ - see front matter © 2012 Elsevier B.V. All rights reserved.
http://dx.doi.org/10.1016/j.cplett.2012.05.028

the interior regions. However, it is still unclear how the carrier relaxation dynamics through the defect states are modulated with dimensions of ZnO nanostructures, especially in the context of shape transition from NPs to NRs.

In this work, we have synthesized size-selected ZnO NPs and NRs (with diameters comparable to the largest NPs) using a simple solution route and studied the changes in optoelectronic behaviors upon transformation of spherical to elongated nanostructures. The crystalline and structural morphologies were characterized by XRD and transmission electron microscopy (TEM), which shows the formation of NPs of various diameters and 1D NRs with preferential growth along the [0001] direction. Emission energy dependent time-resolved PL decay measurements on NPs and NRs show that the carrier recombination dynamics involving the trap states are affected by the size and shape of ZnO nanostructures in a very contrasting manner.

2. Materials and methods

2.1. Synthesis of ZnO nanoparticles and nanorods

Colloidal ZnO NPs were synthesized following previously published report with modifications [5]. Briefly, 0.346 g of KOH (Merck 85%) was refluxed in 30 mL of methanol (Spectrochem, Mumbai India 99.8%) at 60 °C for 45–60 min. In a separate mixture, 10 mL electronic grade methanol with 0.192 g $Zn(OAc)_2{\cdot}2H_2O$ (Loba Chemie, 98%) was prepared. The zinc acetate precursor was then added to the refluxing KOH solution maintained at 60 °C and was stirred vigorously for 3 h. The colloidal NCs were then precipitated and washed thoroughly with Millipore water and then vacuum dried at 30 °C overnight. ZnO NRs were synthesized using a two steps procedure: first, NPs were prepared as prescribed above, but were allowed to grow only for 1 h. Second, an equimolar (1 mM) mixture of zinc nitrate hexahydrate ($Zn(NO_3)_2{\cdot}6H_2O$) (Merck, 96%) and hexamethylenetetramine ($C_6H_{12}N_4$) (Analytical Rasayan, S.D Fine-Chem Limited, 99.5%) was prepared in Millipore water. Sixty milliliters of this complex mixture was then directly added to 2 ml as-prepared ZnO sols in Teflon lined autoclave. The autoclave was sealed and heated at 105 °C for 4 h and then cooled at room temperature overnight. For synthesis of larger NRs, the temperature of the autoclave was raised to 120 °C and was kept heated for 6 h. The precipitated sample was centrifuged, washed several times with Millipore water, and vacuum dried at 30 °C for 24 h. The ZnO nanostructures produced can be re-dispersed in methanol for TEM and other optical measurements.

2.2. Structural characterization

The powder X-ray diffraction (XRD) was performed on a Philips powder diffractometer PW3040/60 with CuK_α radiation (λ = 1.5418 Å). The 2θ angle used in the measurement was 10–70°. The size and morphology of all the products were determined using a field emission gun transmission electron microscopy (TEM) (JEOL-JEM 2100) at an accelerating voltage 200 kV. UV–vis absorption spectra were recorded using a JASCO-V530 absorption spectrophotometer. The steady-state photoluminescence spectra were recorded by fluorescence spectrophotometer (Varian Carry with Eclipse) using an excitation wavelength 325 nm.

2.3. Time-resolved photoluminescence spectroscopy

Time-resolved PL (TRPL) measurements were performed on a time correlated single photon counting (TCSPC) system (IBH, UK) at room temperature in solution in a 1 cm quartz cuvette. The excitation wavelength was 295 nm (Nano LED 295) with the detector response less than 750 ps. The PL decays were collected with an emission polarizer at a magic angle (54.7°) and analysed using IBH DAS 6.2. The data was best fitted biexponentially using the iterative reconvolution method: $I(t) = a_1 \exp(-t/\tau_1) + a_2 \exp(-t/\tau_2)$ where $\sum a_i$ is normalized to unity. The noise is of Poissonian statistics for TRPL obtained by TCSPC technique, and the numerical fit with reduced $\chi^2 \leqslant 1.2$. The residuals (data not shown) are of random noise distributed around zero, indicating good bi-exponential fits.

3. Results and discussion

3.1. Growth and morphology of ZnO nanocrystals

Figure 1a shows the TEM image of nearly spherical ZnO NPs of diameters 6–9 nm with mean particle sizes 7.5 nm. The size distribution from TEM is shown in Figure 1b along with a high-resolution TEM (HR-TEM) image (inset) indicating nearly spherical nature of NPs. The TEM image of NRs (Figure 1c) shows that the diameter between 8 and 11 nm, while length varies from 25–50 nm. The mean diameter (d) of the NRs is ~9.5 nm as obtained from the TEM diameter distribution (Figure 1d). The HR-TEM image (inset of Figure 1d) of ZnO NR show lattice fringes with inter planner distance of ~0.26 nm (shown using arrows), indicating that (002) plane is the preferred growth direction for NRs formation [21]. XRD patterns of both ZnO NPs and NRs (Figure 1e) are found to be consistent with HR-TEM data and all the diffraction peaks are indexed to hexagonal Wurtzite phase. From Figure 1e, it is clear that upon transition from spherical NPs to NRs, the (002) plane becomes more prominent. Moreover, the relative line-width of (002) peak decreases continuously from NPs to NRs (i.e., with increasing aspect ratio, l/d, where l and d is the length and diameter of the NRs, respectively), which indicates a preferential growth process along the polar c-axis, *i.e.*, [0001] direction. This anisotropic growth of the NRs along the c-axis has been explained by oriented-attachment kinetics of NP aggregation where spontaneous self-organization of adjacent particles occurs such a way that they share a common crystallographic orientation followed by joining of these particles at planar interface [23,24].

3.2. Steady state absorption and photoluminescence

The optical absorption and PL spectra of ZnO NPs and NRs dispersed in methanol are shown in Figure 2a and b, and the corresponding spectral peak positions are listed in Table 1. From the absorption spectra of NPs as well as NRs, it is evident that excitonic absorption maxima are blue-shifted from their bulk counterpart (~370 nm), indicative of a weak quantum-confinement. The PL emission spectra of ZnO NCs consist of two emission bands: a sharp transition in the UV and a broad band in the visible range (400–700 nm), the peak positions for both of which red-shift systematically with NC dimensions (Table 1). The narrow UV emission band is due to excitonic recombination of electrons near the conduction band with holes near the valence band. Smaller ZnO NPs (2–5 nm diameters) show an intense defect mediated visible emission (typically quantum yield of ~0.1) along with a very weak NBG transition (Figure 2a, inset). However, for NPs beyond ~8 nm diameters, there is a significant enhancement of the UV transition efficiency and concomitant reduction of the visible emission quantum-yield (~0.05). On transition from NPs to NRs (with similar diameters), the relative intensity of visible emission is further lowered with simultaneous enhancement of the excitonic band. This effect is more pronounced for longer NRs with a higher aspect ratio (Figure 2b, inset). Such a dramatic reduction of the visible emission intensity for the NR suggests that the density of defects

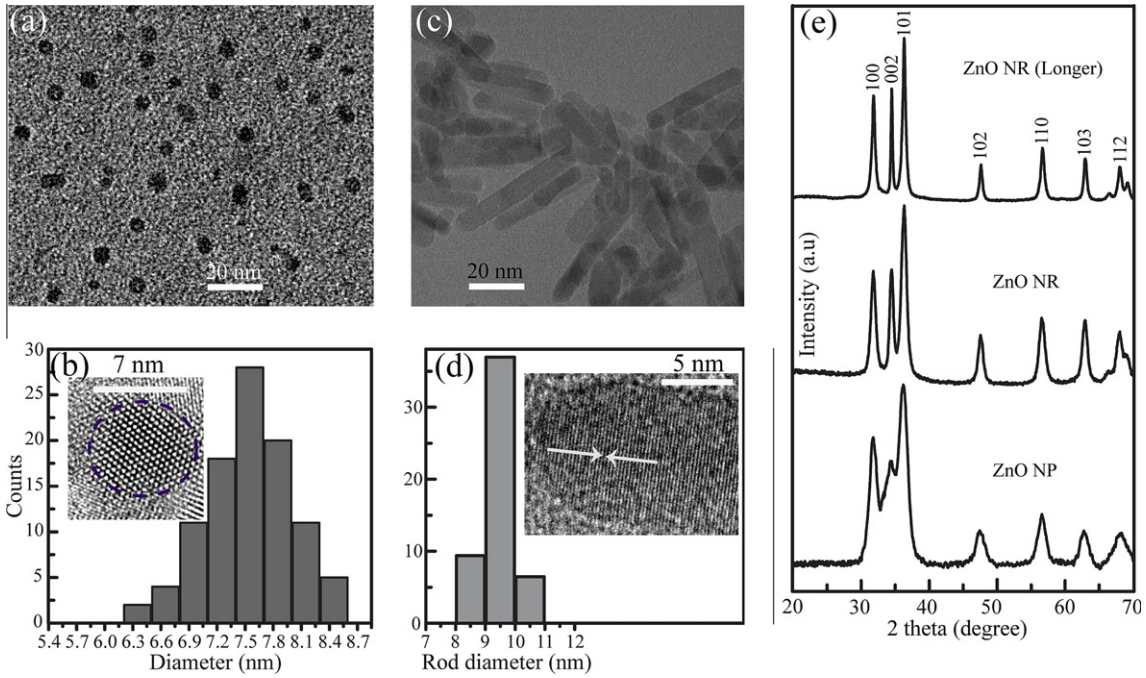

Figure 1. Characterization of ZnO NPs and NRs. TEM images of (a) spherical ZnO NPs, (b) elongated ZnO NRs. TEM diameter distributions for (c) NPs and (d) NRs along with HR-TEM images (insets) showing lattice fringes. The inter-planar distance for NRs is ~0.26 nm (marked using arrows) indicating preferential growth along [0001] direction. (e) XRD patterns of NPs (bottom panel), NRs with l/d ~2–5 (middle panel) and $l/d > 5$ (upper panel), showing both ZnO NPs and NRs have wurtzite structure.

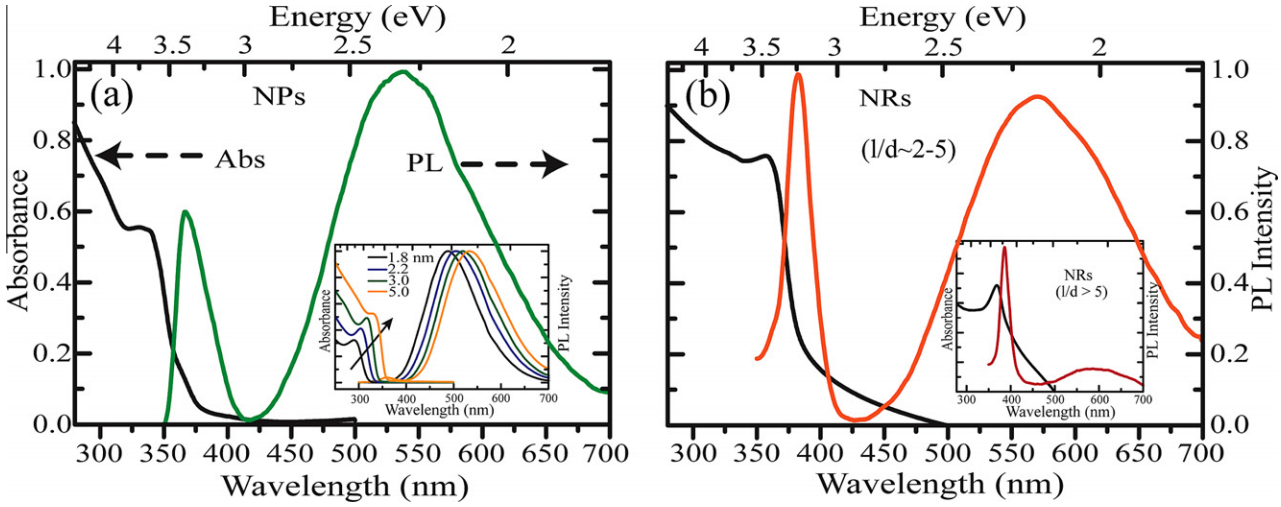

Figure 2. Steady-state optical absorption and PL emission spectra (normalized) of (a) ZnO NPs and (b) ZnO NRs. Changes in the absorption and emission spectra with variation in (a) NP size and (b) for NRs of higher aspect ratio ($l/d > 5$) are shown in the inset.

Table 1
Absorption and emission maxima for ZnO NPs and NRs in methanol.

Mean particle diameter (nm)	λ_{max}(Abs.) (nm)	λ^{em}_{max}(UV) (nm)	λ^{em}_{max}(Vis) (nm)
1.8	290	–	488
2.2	305	–	505
3.0	316	340	520
5.0	330	358	534
8.0	336	367	538
Nanorod aspect ratio (l/d)			
2–5	357	382	570
5–8	368	386	586

is considerably lowered for the NRs. Moreover, both the UV and visible PL emission envelope show a red-shift for NRs as compared to NPs, which is ascribed to band-gap reduction as NPs coarsen to longer NRs. Therefore, the size, shape (or aspect ratio, l/d) and defect densities play an important role in controlling the energies and intensities of the visible emission of ZnO NCs.

In principle, the low energy (visible) trap emission could originate from either surface defects (i.e., dangling bonds, hydroxyl groups) or imperfection in the crystals lattice including extrinsic (impurities) and intrinsic lattice defects (point defects etc.). For instance, the visible PL emission has been ascribed to the presence of native defect centers such as zinc vacancy (V_{Zn}), zinc interstitial (Zn_i), oxygen vacancy (V_o^+), oxygen interstitial (O_i), anti site oxygen (O_{Zn}) etc., as well as to surface related defects as mentioned earlier [11,25–27]. Nonetheless, all these trap states lie within the valence and conduction band of ZnO and significantly influences the carrier relaxation dynamics within the NCs [19].

Although the relative intensity of the visible emission reduces with increasing particle size, the red-shift of the entire emission envelope indicates that the defect energy levels shift alongside the valence and conduction bands with the extent of quantum confinement (i.e. with particle size). Recent studies have shown that this visible luminescence in ZnO is intrinsically broad near single-particle levels [5]. This suggests that inhomogeneities of defect environment within individual nanostructures, rather than size-variations among NPs (or NRs), are responsible for such a broad visible emission [22]. Therefore, the surface chemistry and shape of the ZnO NCs can be expected to play a crucial role in carrier recombination processes through the defect states.

3.3. Time resolved photoluminescence decay

In order to probe the relaxation pathways of charge carriers in these defect states and how they are affected by the NC size and shape, we have performed emission energy dependent TRPL measurements for ZnO NPs of various diameters as well as for NRs (Figures 3a and 4). The TRPL traces obtained at various emission energies are found to be non-exponential (with multiple decay components) and needed hundreds of nanoseconds for complete deactivation, indicating the deep trap nature of the defect states. However, for both NPs and NRs, the decay traces collected up to ~50 ns could be fit to bi-exponential functions, with well separated time constants. Therefore, we focus on the initial PL decay dynamics up to ~50 ns. The parameters (τ_1, a_1, τ_2, a_2) derived from the analyses of TRPL data for NPs and NRs is shown in Figure 3b and Tables 2a and b.

First, TRPL decay traces were collected at a particular wavelength (λ_{em} = 520 nm) for different spherical ZnO NPs (Figure 3a). These measurements show that the PL decay gradually becomes slower as the NP sizes increase from ~1.8 to 5 nm, while there is negligible change in decay profiles for NPs larger than ~5 nm. Figure 3b shows the variation of the two decay components (τ_1 and τ_2) and their relative contributions (a_1 and a_2) as a function of NP diameters. Both the decay components (filled symbols) are found to increase with increasing particle size, and shows saturation tendencies at the weak confinement regimes (d > 5 nm). However, the relative contributions (a_1 and a_2, open symbols) for the fast (τ_1) and slow (τ_2) component show a reverse trend. For the smallest NPs (d ~2 nm) the contribution from τ_1 is dominant, while the slow component becomes major contributing for large NPs (d > ~4 nm). Unambiguous assignment of τ_1 and τ_2 to recombination processes with distinct transition energies is non-trivial because of continuous distribution of sub-band trap states and changing defect density with NP diameters. Nonetheless, the faster PL decay for the smallest NPs (~1.8 nm) and its sensitivity towards slight increment of particle diameters from ~2 to 3 nm is

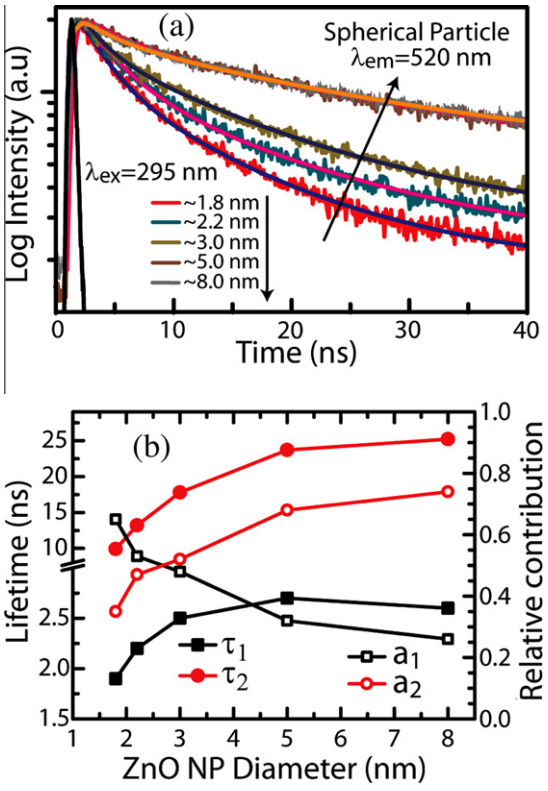

Figure 3. (a) TRPL decay of spherical size-selected spherical ZnO NPs and the best fit (smooth solid lines) to the experimental data using a biexponential function. (b) The variation of the PL lifetime components (filled symbols) and corresponding relative contributions (open symbols) plotted as a function NP diameters.

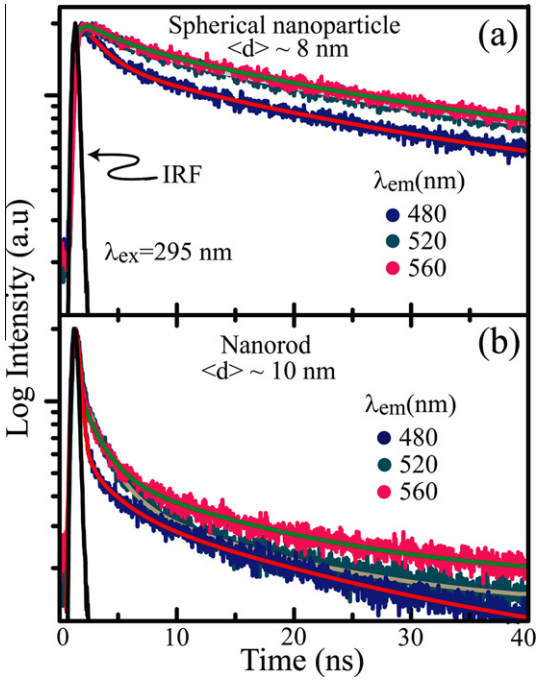

Figure 4. Emission energy dependent TRPL decay traces of (a) ZnO NPs (d ~8 nm) and (b) ZnO NRs (d ~10 nm, l/d ~2–5) dispersed in methanol. The smooth solid lines represent the best fits to the PL decay using a biexponential function. IRF represents the instruments response function.

Table 2a
PL Decay parameters of ZnO NPs (d ~8 nm) dispersed in methanol.

λ_{em} (nm)	τ_1 (ns)	a_1	τ_2 (ns)	a_2	χ^2
480	2.1	0.48	24.8	0.52	1.15
520	2.6	0.26	25.2	0.74	1.12
560	2.8	0.23	26	0.77	1.10

Table 2b
PL Decay parameters of ZnO NRs (l/d ~2–5) dispersed in methanol.

λ_{em} (nm)	τ_1 (ns)	a_1	τ_2 (ns)	a_2	χ^2
480	1.5	0.57	14.2	0.43	1.01
520	1.8	0.87	15.4	0.13	1.02
560	1.9	0.91	16.3	0.09	1.10

indicative of strong coupling between the excitons and surface defect states in the strong confinement regime ($d \leqslant 2a_0$, where a_0 is exciton Bohr radius). The continuous increase of PL lifetimes with increasing NP diameters (2–5 nm) is likely due to dramatic reduction in this coupling as the diameters become larger than exciton Bohr diameter [28]. Moreover, the PL decay traces being unaffected by particle diameters beyond ~5 nm is consistent with the ZnO in weak confinement regimes ($d \gg 2a_0$) where the energetic dependence of particle diameters is also negligible.

To provide insight into the effect of shape transition from spherical to 1-D NCs, emission energy dependent TRPL traces (Figure 4a and b) were obtained for the largest NPs (~8 nm) and for NRs of comparable diameter (~10 nm). Contrary to expectations, the PL decay for the NRs is considerably faster than that of the NPs at all the emission energies, which is also reflected in the evaluated decay parameters (Table 2). Interestingly, the faster PL decay for the NRs is not due to lower values of times constants; τ_1 is similar and τ_2 is slightly lower for NRs (~15 ns) as compared to NPs (~25 ns). Rather, the contributions (a_1 and a_2) to the time-constants are considerably different for NPs and NRs, more so at lower emission energies (520 and 560 nm). In addition, there is nominal energy dependent variation of time-constants for both NPs and NRs, while the respective contribution factors change substantially and show a reverse trend. For NPs, a_1 and a_2 are comparable (~50%) at λ_{em} = 480 nm, while a_2 is larger (~77%) at lower emission energy (λ_{em} ~560 nm). However, contrasting emission energy dependence is observed for the NRs; the fast component (τ_1) is always found to be the preferred recombination channel, the contribution for which becomes overwhelming at lower emission energies (520 and 560 nm). Therefore, the TRPL results demonstrate that: (1) with increasing size (d ~2–8 nm) of spherical NPs, PL decay become considerably slower, (2) the PL decay for the NRs is faster than NPs of comparable diameters, irrespective of emission energies; (3) the relative contributions from the slow decay component becomes increasingly dominant for the NPs at lower emission energies, while for the NRs, the trend is the reversed.

Following excitation in the band gap, several different transitions are responsible for trap emission: (*i*) donor recombination with a positively charged hole in the valence band ($D–h^+$), (*ii*) acceptor recombination with an electron in the conduction band ($A–e^-$), and (*iii*) recombination between an electron localized on a donor with a hole localized on an acceptor, known as donor acceptor pair. It is observed that with increasing particle size, the emission lifetime increases (Figure 3). For semiconductor NCs, the recombination rate of trapped charge carriers is proportional to the square of wavefunction overlap [28]. For smaller particles charge carriers are closer together and hence more effective wavefunction overlap which results in higher oscillator strength. Therefore, the smaller the nanocrystal size, the faster is the recombination rate. The energy dependence of the recombination rate of trap emission (i.e. faster PL decay at higher energies) has been reported for ZnO and other semiconductor NCs, which is attributed to strong Coulomb force between charge carriers [29].

For ZnO NCs, trap emission has two distinct time constants as evaluated from the TRPL data (Table 2). The faster decay component (τ_1) is either due to radiative recombination of shallowly trapped electrons and deep trap holes or due to the recombination of donor acceptor pair. When the PL decay of the two ZnO nanostructures is compared, it is found that the decay for ZnO NPs was slower than that for the ZnO NRs. This may be ascribed to more efficient trapping of the charge carriers due to high density of defects in NPs. This is likely because of higher surface to volume ratio (s/v) in NPs compared to that of NRs. Moreover, variations in defect concentrations and surface states can occur for ZnO NRs [3] and as a result, the internal bulk defect density will be more for NRs than the NPs. It is possible that these internal bulk defects are responsible for faster trapping and de-trapping of electron and as a consequence faster radiative recombination rates in NRs.

Alternatively, anisotropic shape effect of ZnO NRs can also lead to the faster PL decay. It has been reported that splitting of excitonic energy levels occur upon change in aspect ratio of nanocrystals, i.e. upon transition from spherical particles to elongated rods [30–31]. Recently, Kar et al. [32] have shown that surface-defect related PL for SnO_2 NCs show similar relaxation dynamics as observed in our measurements, i.e., a faster PL decay is observed for NRs (~25 nm diameters) as compared to NPs which has been ascribed to shape changes of the NCs. It is therefore plausible that for ZnO NCs, topological surface states will arise from the removal of degeneracy upon transition from spherical NPs to NRs. It is noted that the surface states are known to be strongly dependent on the surface curvature variations which lead to localization of new states along the surface [30,33]. Moreover, for the cylindrical shape NCs the carrier motion is free along the long axis [30], whereas the carrier may be trapped on an undulating surface. Hence, lowering of symmetry in ZnO NRs as compared to spherical NPs might lead to the fast decay dynamics as observed in our experiments.

4. Conclusions

Our results show that size and shape of quantum-confined ZnO nanostructures influence the carrier recombination dynamics involving defect states in a very contrasting manner. The PL decay becomes slower with increasing NP size and shows saturation tendency in the weak-confinement regimes (d ~6 nm). These changes in the lifetime components and their relative contributions are likely to be due to reduction in coupling between the exciton and the surface defect states upon increasing particle size from 2 to 6 nm. However, the carrier recombination dynamics through the defect states for NRs is found to show an opposite trend and become considerably faster as compared to NPs of similar diameters. The differences in emission energy dependent dynamics for either NPs or NRs are found not to be due to pronounced change in the lifetime components. Rather, the relative contributions to the radiative lifetimes are altered dramatically; for NPs the slower pathway is the preferred recombination channel, while it is the reverse for NRs. This is likely to be due to manifestation of topological surface states and alteration in defect densities for the anisotropic NRs.

Acknowledgements

We would like to thank Centre for Research in Nanotechnology and Science (CRNTS) for TEM facility, and Departments of Chemistry, IIT Bombay for usage of central facility instruments. We acknowledge a CSIR (India) grant to AC (Scheme: 80(0070)/08/EMR-II) and IRCC IIT Bombay for partial support of this work and PhD scholarship to AL. We acknowledge support of the Ministry of New and Renewable Energy (MNRE), Government of India.

References

[1] G.R. Li, T. Hu, G.L. Pan, T.Y. Yan, X.P. Gao, H.Y. Zhu, J. Phys. Chem. C 112 (2008) 11859.
[2] M.H. Huang et al., Science 292 (2001) 1897.
[3] Y. Zhong, A.B. Djurisic, Y.F. Hsu, K.S. Wong, G. Brauer, C.C. Ling, W.K. Chan, J. Phys. Chem. C 112 (2008) 16286.
[4] A.B. Djurisic, Y.H. Leung, W.C.H. Choy, K.W. Cheah, W.K. Chan, Appl. Phys. Lett. 84 (2004) 2635.
[5] A. Layek, S. De, R. Thorat, A. Chowdhury, J. Phys. Chem. Lett. 2 (2011) 1241.
[6] H. He, Q. Yang, C. Liu, L. Sun, Z. Ye, J. Phys. Chem. C 115 (2011) 58.
[7] A.B. Djurisic, Y.H. Leung, Small 2 (2006) 944.
[8] N.S. Norberg, D.R. Gamelin, J. Phys. Chem. B 109 (2005) 20810.
[9] D.S. Bohle, C.J. Spina, J. Am. Chem. Soc. 129 (2007) 12380.

[10] L. Irimpan, V.P.N. Nampoori, P. Radhakrishnan, A. Deepthy, B. Krishnan, J. Appl. Phys. 102 (2007) 063524.
[11] D. Bera, L. Qian, S. Sabui, S. Santra, P.H. Holloway, Opt. Mater. 30 (2008) 1233.
[12] R.C. Lima et al., J. Phys. Chem. A 112 (2008) 8970.
[13] L. Zhang, L. Yin, C. Wang, N. lun, Y. Qi, D. Xiang, J. Phys. Chem. C 114 (2010) 9651.
[14] I. Shalish, H. Temkin, V. Narayanamurti, Phys. Rev. B 69 (2004) 245401.
[15] S. Lettieri, L.S. Amato, P. Maddalena, E. Comini, C. Baratto, S. Todros, Nanotechnology 20 (2009) 175706.
[16] M.J.S. Spencer, Prog. Mater Sci. 57 (2012) 437.
[17] D. Chu, Y. Masuda, T. Ohji, K. Kato, Langmuir 26 (2010) 2811.
[18] Y. Darici, P.H. Holloway, J. Sebastian, T. Trottier, S. Jones, J. Rodriquez, J. Vac. Sci. Technol. A 17 (1999) 692.
[19] H.J. Queisser, E.E. Haller, Science 281 (1998) 945.
[20] M.A. El-Sayed, Acc. Chem. Res. 37 (2004) 326.
[21] G. Pozina, L.L. Yang, Q.X. Zhao, L. Hultman, P.G. Lagoudakis, Appl. Phys. Lett. 97 (2010) 131909.
[22] B.P. Mehl, J.R. Kirschbrown, R.L. House, J.M. Papanikolas, J. Phys. Chem. Lett. 2 (2011) 1777.
[23] C. Pacholski, A. Kornouski, H. Weller, Angew. Chem. Int. Ed. 41 (2002) 1188.
[24] M. Ethayaraja, R. Bandyopadhyaya, Langmuir 23 (2007) 6418.
[25] S. Rakshit, S. Vasudevan, J. Phys. Chem. C 112 (2008) 4531.
[26] A. van Dijken, E.A. Meulenkamp, D. Vanmaekelbergh, A. Meijerink, J. Lumin. 90 (2000) 123.
[27] A. van Dijken, E.A. Meulenkamp, D. Vanmaekelbergh, A. Meijerink, J. Phys. Chem. B 104 (2000) 1715.
[28] N.T.D. Chestnoy, R.H. Harris, L.E. Brus, J. Phys. Chem. 90 (1986) 3393.
[29] P.V. Kamat, B. Patrick, J. Phys. Chem. 96 (1992) 6829.
[30] M.B. Mohamed, C. Burda, M.A. El-Sayed, Nano Lett. 1 (2001) 589.
[31] J. Li, L.W. Wang, Nano Lett. 3 (2003) 1357.
[32] A. Kar, S. Kundu, A. Patra, J. Phys. Chem. C 115 (2011) 118.
[33] S. Sadhu, A. Patra, J. Phys. Chem. C 115 (2011) 16867.